AIAA JOURNAL
Vol. 49, No. 6, June 2011

Technical Notes

Adjoint-Based Shape Optimization for Electromagnetic Problems Using Discontinuous Galerkin Methods

Li Wang* and W. Kyle Anderson†
University of Tennessee at Chattanooga, Chattanooga, Tennessee 37403

DOI: 10.2514/1.J050594

Introduction

IN RECENT years, discontinuous Galerkin (DG) methods have received considerable attention for solving a wide range of convection-dominated problems, such as in computational fluid dynamics [1] and electromagnetics [2]. The main benefits of using the DG methods arise from their capability to obtain optimal error convergence rates and suitability for efficient parallel computing. Because sensitivity analysis techniques have become an indispensable component of the design process, the DG method has also been extended to provide sensitivity derivatives for both steady-state and time-dependent flows. As an example, a discrete adjoint approach for unsteady flow problems is described in [3] for a high-order DG method discretized on unstructured curvilinear meshes.

The purpose of the work presented in this paper is to apply the research described in [3,4] for electromagnetic problems. The accuracy of the DG scheme is examined to demonstrate that the design order is achieved through fifth-order accuracy. A time-dependent discrete adjoint method is also employed to obtain sensitivity derivatives, which are subsequently coupled with a formal optimization procedure to determine the shape of an airfoil to obtain a desired magnetic field on the airfoil surface over a specified period of time.

Equations and Discretizations

The following conservative form of the two-dimensional source-free Maxwell equations is considered:

$$\frac{\partial \mathbf{q}(\mathbf{x},t)}{\partial t} + \frac{\partial \mathbf{F}(\mathbf{q}(\mathbf{x},t))}{\partial x} + \frac{\partial \mathbf{G}(\mathbf{q}(\mathbf{x},t))}{\partial y} = 0 \tag{1}$$

where $\mathbf{q}$, $\mathbf{F}$ and $\mathbf{G}$ are given by

$$\begin{aligned} &\mathbf{q} = \{D_x, D_y, B_z\}^T, \\ &\mathbf{F} = \{0, B_z/\mu, D_y/\varepsilon\}^T \quad \text{and} \quad \mathbf{G} = \{-B_z/\mu, 0, -D_x/\varepsilon\}^T \end{aligned} \tag{2}$$

or

$$\begin{aligned} &\mathbf{q} = \{B_x, B_y, D_z\}^T, \\ &\mathbf{F} = \{0, -D_z/\varepsilon, -B_y/\mu\}^T \quad \text{and} \quad \mathbf{G} = \{D_z/\varepsilon, 0, B_x/\mu\}^T \end{aligned} \tag{3}$$

for a transverse-electric (TE) mode or a transverse-magnetic (TM) mode, respectively. Here, ε and μ denote the relative permittivity and permeability, respectively, and are both assumed to be unity for the present work. The discontinuous Galerkin weak formulation to this problem is written as

$$\int_{\Omega_k} \phi_j \frac{\partial \mathbf{q}_p}{\partial t}\,\mathrm{d}\Omega_k - \int_{\Omega_k} \left[\frac{\partial \phi_j}{\partial x}\mathbf{F}(\mathbf{q}_p) + \frac{\partial \phi_j}{\partial y}\mathbf{G}(\mathbf{q}_p)\right]\mathrm{d}\Omega_k + \int_{\partial\Omega_k} \phi_j \mathbf{H}(\mathbf{q}_p^+, \mathbf{q}_p^-, \mathbf{n})\,\mathrm{d}S = 0 \tag{4}$$

for each element (e.g., k) in the computational domain; $\mathbf{q}_p$ represents the Galerkin solution approximation, which is expanded as a series of modal solution coefficients and hierarchical basis functions $\{\phi_i\}$ [4], expressed as $\mathbf{q}_p = \sum_{i=1}^{M} \tilde{\mathbf{q}}_{p_i}\phi_i(\mathbf{x})$. The flux on the elemental boundaries, $\mathbf{H}(\mathbf{q}_p^+, \mathbf{q}_p^-, \mathbf{n})$, is determined from the data on either side of the interface using a Riemann flux function similar to that described in [5]. For edges coinciding with physical boundaries, a perfectly conducting wall condition is applied, where the tangential components of the electric field vanish. For evaluating the integrals in Eq. (4), isoparametric elements are used and an appropriate number of quadrature points are used to accurately approximate the volume and surface integrals.

Equation (4) can be written as an ordinary differential equation in time, which is integrated using an implicit, second-order backward difference formula (BDF2) [4].

Adjoint-Based Sensitivity Analysis

During a design cycle, surface nodes and quadrature points are repositioned through the superposition of Hicks–Henne functions [6] placed at a predesignated set of surface nodes. The design variables $\mathbf{D}$ correspond to the magnitude of the Hicks–Henne functions and are continuously updated throughout the design process. As the surface definition evolves, the interior mesh points are deformed using a linear spring analogy [7] to prevent the generation of overlapping elements. As a consequence, proper computation of the mesh sensitivities requires that the effects due to the relocation of both grid points and quadrature points be accounted for. The discrete adjoint sensitivity formulation is shown in Eqs. (5) and (6), while a detailed derivation of the procedure is given in [3]

$$\left(\frac{\mathrm{d}L}{\mathrm{d}\mathbf{D}}\right)^T = \left(\frac{\partial \mathbf{x}_s}{\partial \mathbf{D}}\right)^T \lambda_x + \left(\frac{\partial \mathbf{x}_q}{\partial \mathbf{D}}\right)^T \left(\frac{\partial \tilde{\mathbf{x}}}{\partial \mathbf{x}_q}\right)^T \left(\frac{\partial \bar{L}}{\partial \tilde{\mathbf{x}}}\right)^T \tag{5}$$

where

$$\left(\frac{\partial \bar{L}}{\partial \tilde{\mathbf{x}}}\right)^T = \left(\frac{\partial L}{\partial \tilde{\mathbf{x}}}\right)^T - \sum_{n=1}^{N} \left(\frac{\partial \bar{\mathbf{R}}_e^n}{\partial \tilde{\mathbf{x}}}\right)^T \lambda_q^n \tag{6}$$

In the equations, L refers to a scalar-valued objective functional for minimization; $\mathbf{x}_s$ and $\mathbf{x}_q$ refer to coordinates of surface grid points and surface quadrature points; $\tilde{\mathbf{x}}$ denotes the element-based geometric mapping coefficients; $\mathbf{R}_e$ represents the unsteady residual vector and K refers to the mesh stiffness matrix [7]; λ_x and λ_q are the computed mesh adjoint and primal-adjoint variables [3], respectively. N denotes the total number of time steps, and $\partial \bar{\mathbf{R}}_e^n / \partial \tilde{\mathbf{x}}$ denotes the sensitivities of the unsteady residual in time step n with respect to the mesh configuration and is obtained by

Received 6 April 2010; revision received 14 January 2011; accepted for publication 25 January 2011.

*Research Assistant Professor, SimCenter: National Center for Computational Engineering, 701 E. M. L. King Blvd. Member AIAA.

†Professor, SimCenter: National Center for Computational Engineering, 701 E. M. L. King Blvd. Associate Fellow AIAA.

$$\frac{\partial \bar{\mathbf{R}}_e^n}{\partial \tilde{\mathbf{x}}} = \frac{\partial \mathbf{R}_e^n}{\partial \tilde{\mathbf{x}}} + \left[\frac{\partial \mathbf{R}_e^n}{\partial \mathbf{q}_b^n}\right] \frac{\partial \mathbf{q}_b^n}{\partial \tilde{\mathbf{x}}} + \sum_{k=1}^{2} \delta_{kn} \left[\frac{\partial \mathbf{R}_e^n}{\partial \tilde{\mathbf{q}}^0}\right] \frac{\partial \tilde{\mathbf{q}}^0}{\partial \tilde{\mathbf{x}}} \tag{7}$$

for the BDF2 scheme employed in this work; δ represents the Kronecker-delta operator. Note that the last term in Eq. (7) arises from the mesh dependence of a specified initial condition and has contributions only from the first and second time steps (in the BDF2 scheme). Since typical applications of sensitivity analysis have uniform freestream initial conditions, this term has not been previously included. However, it must be evaluated when a non-uniform initial condition is applied, as the omission could lead to inaccuracy in the sensitivity derivatives.

The current work employs the portable, outstanding, reliable, and tested (PORT) trust region optimization strategy [8] to obtain a new set of design variables. The primary cost of one design iteration arises from the solutions of the electromagnetic field and adjoint equations, which are roughly equivalent for the design case considered in the present work. The total cost for any design depends on the physical problem, the number and type of design variables and the acceptable convergence level.

Numerical Examples

Before demonstrating the design capability, a study is first conducted to verify that the spatial accuracy of the implemented scheme is consistent with the design order. For this test, a scattering problem with an analytical solution [9] is considered where a transverse-magnetic field, with a nondimensional frequency of 3.5, impacts a circular cylinder. At the surface of the cylinder a perfect electric conductor boundary condition is applied, whereas the time-dependent analytical solution is imposed as a Dirichlet condition at the outer boundary. Three grids, consisting of 602, 1433, and 3033 triangles, are used to evaluate the spatial error convergence of the DG scheme for polynomial orders ranging from $p = 1$ to $p = 4$. Contours of the y-component of the magnetic flux density computed using the fifth-order DG scheme are compared with the exact solution in Fig. 1a. It is seen that the solution computed with the DG scheme (dashed lines) agrees qualitatively very well with the exact solution. In Fig. 1b, the L_2 norm of the solution error, computed using all the field variables at $t = 1$, demonstrates that the optimal error convergence rate ($\sim h^{p+1}$) is achieved for all orders of DG discretization. In particular, the asymptotic slopes for the $p = 1$, $p = 2$, $p = 3$, and $p = 4$ DG schemes are 1.99, 3.07, 4.10, and 5.26, respectively. Note that in obtaining these results, the time step for the BDF2 scheme has been chosen sufficiently small to ensure that the spatial error dominates the temporal error. Furthermore, at each time step, an eighth-order-of-magnitude reduction in the L_2 norm of the unsteady residual is obtained using the p-multigrid approach developed in [4].

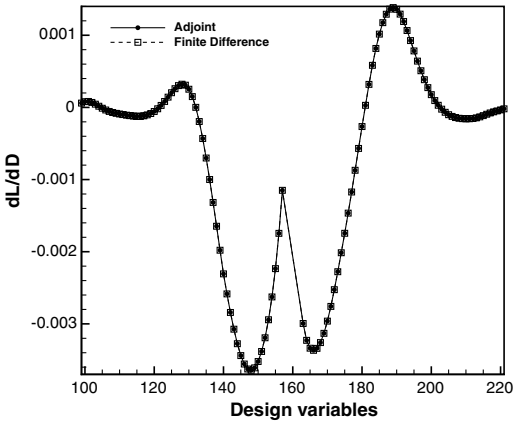

Fig. 2 Comparison of sensitivity derivatives using the unsteady discrete adjoint method and a fifth-order DG scheme with finite difference gradients for the original mesh and airfoil geometry.

The next example considers an unsteady adjoint-based shape optimization case for a TE field scattered by an airfoil. Note that there are no limitations of the methodology specific to an airfoil and that with appropriate parameterizations other applications, such as bandpass filters, power dividers, or other microwave devices, may be considered. The goal of this shape optimization case is to match a time-dependent magnetic flux density profile on the target NACA65 (1)-212 airfoil by changing the shape of the original NACA0012 airfoil geometry. The objective functional is thus defined as

$$L = \sqrt{\frac{\sum_{n=1}^{N} \sum_{i=1}^{N_s} (B_{zi}^n - B_{zi}^{*n})^2}{N \times Ns}} \tag{8}$$

where B_{zi}^n and B_{zi}^{*n} denote the values of the magnetic solution at time step n for surface point i on the respective current and target airfoil surfaces. N and N_s represent the total number of time steps ($N = 150$ in this case) and the number of surface grid points. The domain ranges from -1 to 2 in the x-coordinate direction and -1 to 1 in the y-direction. A computational mesh containing 4367 unstructured triangular elements is employed, along with 118 design variables spanning about 99% of the chord locations on the upper and lower airfoil surfaces. The BDF2 implicit scheme with a time step size of $\Delta t = 8 \times 10^{-3}$ is employed and the unsteady design procedure is

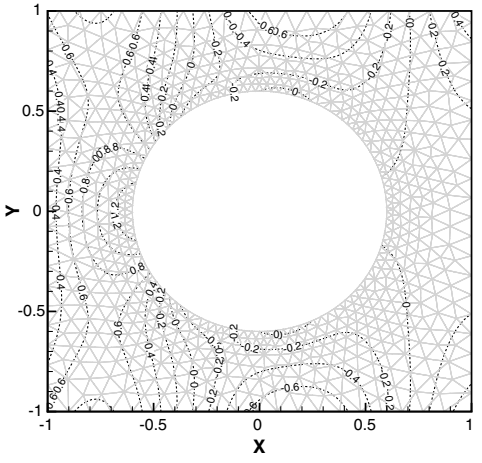

a) Computational mesh and contours of Y-component of the magnetic flux density

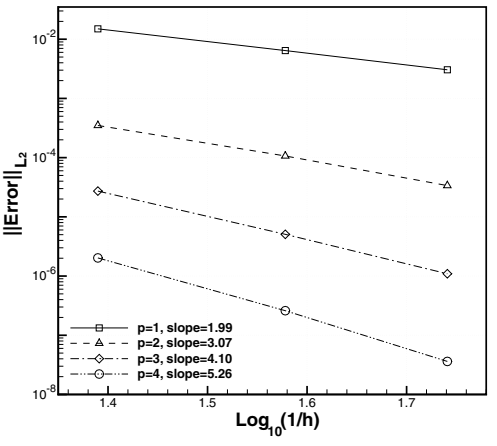

b) Spatial error vs. grid spacing

Fig. 1 TM wave scattered by a perfectly conducting circular cylinder: a) computational mesh (containing 1433 elements) and comparison of B_y contours with the exact solution at $t = 1$ using a $p = 4$ spatial DG discretization and the BDF2 scheme, and b) convergence of the solution error for various discretization orders ($1 \le p \le 4$) as a function of grid spacing.

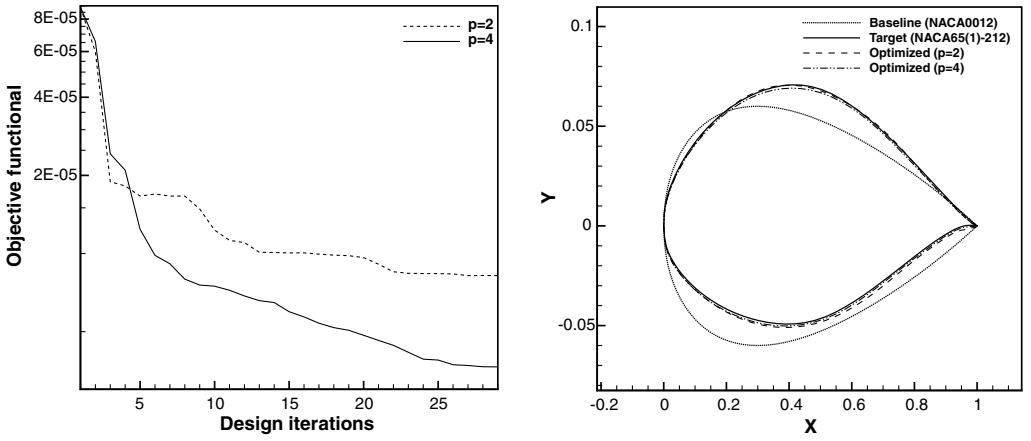

a) Functional convergence **b) Comparison of airfoil shapes**

Fig. 3 Electromagnetic shape optimization for a TE field scattered by an airfoil using various orders of DG discretizations: a) convergence of the objective functional in terms of the number of design iterations, and b) comparison of airfoil shapes using an exaggerated scale.

performed using the third-order ($p = 2$) and fifth-order-accurate ($p = 4$) DG spatial schemes. A time-harmonic TE mode with a nondimensional angular frequency of $\alpha = 20$ is prescribed ahead of the airfoil (for $x < -\pi/2\alpha$) and is allowed to propagate downstream in the x-coordinate direction. Note that the use of nonuniform initial conditions requires the inclusion of the last term in Eq. (7). The airfoil surface is treated as a perfect electric conductor and the time-dependent electromagnetic solution for a streamwise propagating TE wave is imposed on the outer boundaries. The unsteady primal and adjoint problems are solved with four or five p-multigrid iterations at each time step, leading to approximately a seven order-of-magnitude reduction in the unsteady residual. Validation of the sensitivity calculation using the adjoint method is illustrated in Fig. 2 for the $p = 4$ DG scheme by comparing with finite difference gradients, where an excellent match is observed. Figure 3a plots the convergence of the objective functional against the number of design cycles, using the third-order- and fifth-order-accurate DG schemes. Over a one-order magnitude reduction in the objective is obtained in 20 steps for both spatial schemes, although the fifth-order scheme attains 30% greater reduction than the third-order scheme. Figure 3b compares the geometry shapes for the original, target and final optimized airfoils in an exaggerated scale for both $p = 2$ and $p = 4$ DG spatial schemes. It is observed that the final airfoil shapes obtained with both schemes are almost identical and match the target geometry very well, with a maximum deviation from the target of about 7% for the $p = 2$ scheme, and 3% for the $p = 4$ scheme. The close agreement between the results obtained using the two schemes demonstrates that the final geometry is not greatly influenced by discretization error and that further increases in either the order of accuracy or refinement of the mesh would not produce significant changes in the final shape.

Conclusions

This paper presents a discrete adjoint algorithm for computing sensitivity information in electromagnetic shape optimization problems in the context of high-order discontinuous Galerkin discretizations. Convergence of the spatial discretization error has been examined and the optimal error convergence ($\sim h^{p+1}$) is achieved. Third- and fifth-order results demonstrate that the various orders of the DG schemes, in conjunction with the adjoint-based sensitivities, are effective at reducing the cost functional for the electromagnetic scattering design case. For the case considered, greater reduction in objective is obtained by the high-order scheme.

Acknowledgment

The work was supported by the Tennessee Higher Education Commission Center of Excellence in Applied Computational Science and Engineering. The support is greatly appreciated.

References

[1] Bassi, F., Crivellini, A., Pietro, D. A. D., and Rebay, S., "An Implicit High-Order Discontinuous Galerkin Method for Steady and Unsteady Incompressible Flows," *Computers and Fluids*, Vol. 36, No. 10, 2007, pp. 1529–1546. doi:10.1016/j.compfluid.2007.03.012

[2] Hesthaven, J. S., and Warburton, T., "Nodal High-Order Methods on Unstructured Grids. I. Time-Domain Solution of Maxwell's Equations," *Journal of Computational Physics*, Vol. 181, No. 1, 2002, pp. 186–221. doi:10.1006/jcph.2002.7118

[3] Wang, L., Mavriplis, D. J., and Anderson, W. K., "Unsteady Discrete Adjoint Formulation for High-Order Discontinuous Galerkin Discretizations in Time-Dependent Flow Problems," AIAA Paper 2010-367, Jan 2010.

[4] Wang, L., and Mavriplis, D. J., "Implicit Solution of the Unsteady Euler Equations for High-Order Accurate Discontinuous Galerkin Discretizations," *Journal of Computational Physics*, Vol. 225, No. 2, 2007, pp. 1994–2015. doi:10.1016/j.jcp.2007.03.002

[5] Mohammadian, A., Shankar, V., and Hall, W., "Computation of Electromagnetic Scattering and Radiation Using a Time-Domain Finite-Volume Discretization Procedure," *Computer Physics Communications*, Vol. 68, Nos. 1–3, 1991, pp. 175–196. doi:10.1016/0010-4655(91)90199-U

[6] Hicks, R. M., and Henne, P. A., "Wing Design by Numerical Optimization," *Journal of Aircraft*, Vol. 15, No. 7, 1978, pp. 407–412. doi:10.2514/3.58379

[7] Yang, Z., and Mavriplis, D. J., "Unstructured Dynamic Meshes with Higher-Order Time Integration Schemes for the Unsteady Navier–Stokes Equations," AIAA Paper 2005-1222, Jan 2005.

[8] Fox, P. A., Hall, A. D., and Schryer, N. L., "The PORT Mathematical Subroutine Library," ACM TOMS 4, 1978, 104–126.

[9] Harrington, R. F., *Time-Harmonic Electromagnetic Fields*, Wiley Interscience, New York, 2001.

T. Zang
Associate Editor